Available online at www.sciencedirect.com
ScienceDirect
Journal of the European Ceramic Society 28 (2008) 1857–1869
www.elsevier.com/locate/jeurceramsoc

A numerical tool to estimate SOFC mechanical degradation: Case of the planar cell configuration

J. Laurencin [a,*], G. Delette [a], F. Lefebvre-Joud [a], M. Dupeux [b]

[a] *CEA/LITEN/DTH/LEV, 17 avenue des martyrs, 38054 Grenoble, France*
[b] *SIMAP (INP Grenoble/CNRS/UJF), BP 75 38402 Saint Martin d'Hères, France*

Received 27 July 2007; received in revised form 27 November 2007; accepted 9 December 2007
Available online 4 March 2008

Abstract

The stress state and cell degradation have been modelled considering the classical solid oxide fuel cells (SOFCs) materials (Ni–YSZ//YSZ//LSM). The anode-supported cell is found to be un-cracked after its elaboration. However, the high level of energy stored in the thin electrolyte layer lowers the cell robustness as it constitutes the driving force for interfacial delamination. The elaboration of the electrolyte supported cell leads to the anode layer cracking. The heating up to 800 °C and the cermet reduction allow relaxing the stress level in the cell. For the anode-supported cell, the cermet re-oxidation induces cathode damage as soon as the anodic strain exceeds 0.05–0.09% whereas the electrolyte fracture occurs for strain ranging between 0.12% and 0.15%. For the electrolyte supported cell, the cermet re-oxidation induces a triggered risk of anode/electrolyte delamination when the anodic strain is higher than 0.3–0.35%. The risk of rupture initiation in cell singularities has been also investigated. A pure material electrode/electrolyte singularity is harmless. A perpendicular corner at the electrode/electrolyte free edge constitutes a harmful singularity.

Keywords: Failure analysis; Fuel cells; SOFC; Stress singularity

1. Introduction

Solid oxide fuel cells (SOFCs) are devices allowing the conversion of the chemical energy into electricity. As these kinds of fuel cell operate at high temperatures, they present the advantage of high efficiency and large fuel flexibility. For instance, SOFCs are able to oxidize hydrogen, carbon monoxide, methane and potentially other hydrocarbon fuels. The cell or Multiple Electrode Assembly (MEA) is mainly constituted of three ceramic layers: two porous electrodes separated by a dense electrolyte. The usual materials employed for the MEA are yttria-stabilized zirconia (YSZ) for the electrolyte, Ni–YSZ cermet for the anode and strontium-doped lanthanum manganite (LSM) for the cathode.[1] Because of the low mechanical strength and intrinsic brittleness of these materials, the MEA constitutes a critical component regarding to SOFC reliability. Therefore, the mechanical degradation of the cell remains a major limitation to the industrial developments of SOFCs.

The cell is submitted to various kinds of mechanical loading with several origins. Residual stresses arise at room temperature because of the cell manufacturing process. In addition, stresses can appear during SOFC operation: these stresses can be caused by an external loading of the cell in a stack or by a possible thermal gradient. If the fuel supply is accidentally stopped, the cermet re-oxidation may occur. This re-oxidation step generates an anodic bulk expansion which can lead to a high level of stress in the cell layers.

On its edges, the cell presents some material and geometrical singularities where the stress (in principle) tends to infinity.[2] The points A, C, and D in Fig. 1 can be described as a combination of material and geometrical singularities whereas the point B is a pure material singularity. The stress field in such area is the sum of two independent terms: the first one is related to the regular far-range stress field which is dominant in the whole structure except in the singular zone, and the second one is the singular stress field which is only dominant in the vicinity of the singularities. Because of the high stress level reached in the neighbourhood of the singularities, these particular points of the cell structure are potentially harmful for its mechanical integrity.

This work is based on the calculation of stress field arising in planar cell configuration. The two geometrical variants with an

* Corresponding author. Tel.: +33 4 38782210; fax: +33 4 38784139.
E-mail address: laurencin@chartreuse.cea.fr (J. Laurencin).

0955-2219/$ – see front matter © 2008 Elsevier Ltd. All rights reserved.
doi:10.1016/j.jeurceramsoc.2007.12.025

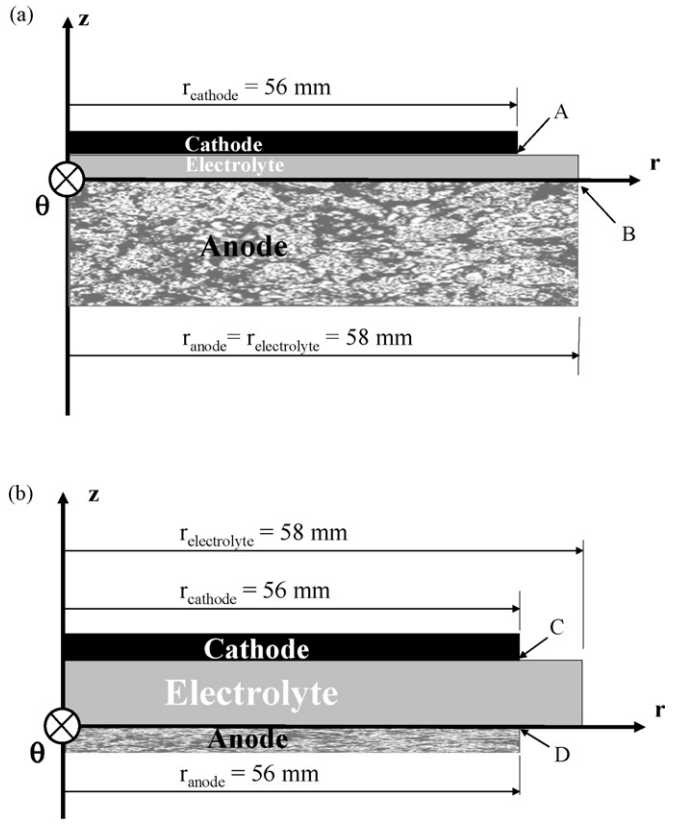

Fig. 1. Axisymmetric representation of the two studied variants of planar cells: (a) anode-supported cell configuration and (b) electrolyte-supported cell configuration.

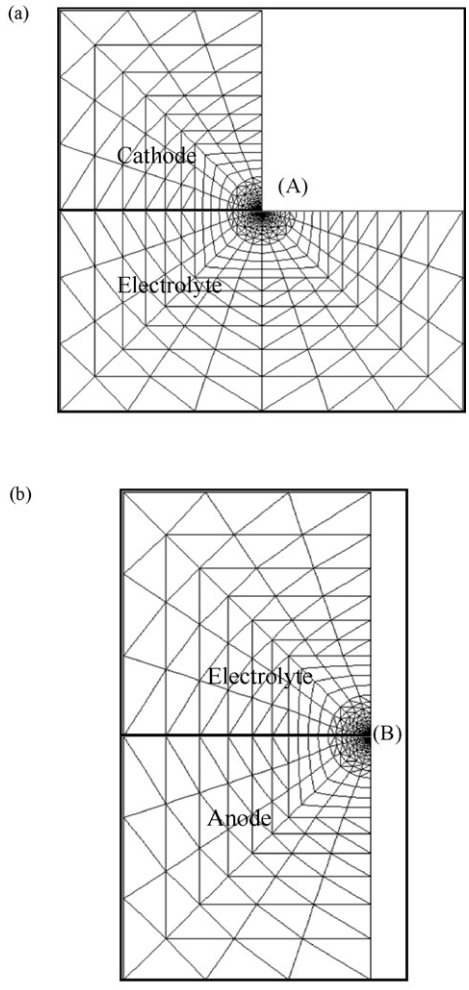

Fig. 2. Mesh refinement at singularities for the anode supported cell configuration: (a) arrangement of elements surrounding the singularity A (see point A in Fig. 1). (b) Arrangement of elements surrounding the singularity B (see point B in Fig. 1).

anode or electrolyte support have been investigated. The stress field has been determined at room temperatures and during cell operation. The effect of anode re-oxidation has also been studied. Then, the risk of cell degradation has been predicted thanks to a statistical approach of failure based on the Weibull theory. The failure probabilities have been calculated for the classical regular stress field. A special attention has also been paid to estimate the risk of damaging induced from singularities.

2. Mechanical models and failure analysis methodology

2.1. General assumptions

The cell geometries considered in the present work exhibit a circular shape with an external diameter equal to 116 mm. In the case of the anode supported cell, the electrolyte and cathode are thin layers deposited onto the anodic substrate: their thicknesses have been chosen as 0.02 and 0.06 mm, respectively. The thickness of the porous anode has been fixed to 1 mm. As illustrated in Fig. 1a, the cathode layer overlaps only partially the electrolyte one. These two layers are assumed to shape an ideal perpendicular corner at the edge of the cell (point A in Fig. 1a).

In the case of the electrolyte-supported cell, the thin electrodes are deposited onto the dense electrolyte. The thicknesses of the MEA layers are 0.150 mm for the electrolyte and 0.06 mm for each of the electrodes. As illustrated in Fig. 1b, the electrode radius is assumed to be smaller than the electrolyte one. The free edge of the cell presents two perpendicular corners between electrodes and electrolyte (points C and D in Fig. 1b).

Owing to the circular geometry of the cell, an axisymmetric numerical analysis has been used (Fig. 1). The stress calculations have been carried out with the software Cast3m[3] based on the finite element method (FEM). The mesh has been designed with 8-node 2D elements. As illustrated in Fig. 2, a mesh refinement has been made in the neighbourhood of the singularities to compute the stress field divergence accurately. The constitutive laws chosen to perform the simulations are representative of a purely elastic behavior for each cell layer. The usual SOFC cell materials have been considered for this study (*i.e.* Ni–YSZ//YSZ//LSM). Their elastic properties are given in Table 1. It is worth noting that the Young's modulus of the anodic cermet heavily depends on the oxidized or reduced state of the nickel phase. The observed decrease in magnitude of elastic modulus is mainly caused by the increase in porosity of the material as a result of NiO reduction.[4,5] Values given in Table 1 correspond to an anodic porosity of 43% in the Ni–YSZ reduced state and a residual porosity of 23% in the NiO–YSZ oxidized state.

Table 1
Elastic properties of each cell material

	Young's modulus (GPa)	Poisson's ratio	Thermal expansion coefficient TEC ($\times 10^{-6}\,^{\circ}C^{-1}$)
NiO–YSZ (oxidized anode)	112.3[4,5]	0.284[4,5]	12.5[a]
Ni–YSZ (reduced anode)	56.8[4,5]	0.258[4,5]	12.5[6]
YSZ (electrolyte)	190.0[7]	0.308[7]	10.8[8,11]
LSM (cathode)	35.0[9]	0.36[10]	11.7[11]

[a] Assumed to be equivalent to Ni–YSZ.

2.2. Stress field simulation

2.2.1. Residual stress calculation at room temperature

It has been assumed that the anode supported cell is stress free at the anode/electrolyte co-sintering temperature, taken here at the usual value of $T = 1350\,^{\circ}C$.[12] The calculated residual stress is then assumed to be only caused by the thermal expansion coefficients (TECs) mismatch between the cell layers and induced by the cooling from 1350 °C to the room temperature.

In the case of the electrolyte-supported cell, the anode is firstly deposited onto the electrolyte substrate and fired at 1350 °C. The LSM cathode is layered in a second step and usually sintered at temperatures ranging from 1100 to 1300 °C.[13,14] These two elaborating steps have been modelled as follows:

(i) Step 1: the thermal residual stress of the anode/electrolyte half-cell is calculated for a cooling from 1350 °C to the room temperature. The risk of the bi-layer cracking and stress relaxation is then evaluated.
(ii) Step 2: the residual stress of the complete MEA is calculated considering a cooling from 1200 °C to the room temperature. This calculation is carried out by accounting the initial loading of the cell (due to the thermal residual stress at 1200 °C of the anode/electrolyte bi-layer).

For both the anode and electrolyte-supported cells, the fabrication process is classically performed under oxidizing atmosphere (air). Consequently, the calculations have been carried out considering the anodic cermet into its NiO–YSZ chemical state.

2.2.2. Stress calculation during cell operation

In the present model, the cell is free to bend and is not constrained in any way by the interconnect plates. This last assumption is realistic if the glass seals maintaining the cell are viscous at high temperature and, hence, introduces no external loading. To estimate the evolution of the cell stress field during operation, the starting process of a SOFC cell has been simulated considering two steps:

(i) Step 1: the cell is heated from room temperature to the SOFC operating temperature ($T = 800\,^{\circ}C$). This temperature increase is performed under oxidizing atmosphere (air). It means that the anodic cermet remains into its NiO–YSZ chemical state.
(ii) Step 2: hydrogen is introduced and NiO is reduced into Ni. Since no shrinkage has been currently reported in open literature during the NiO–YSZ reduction,[15,16] this step has been simulated by taking into account only the decrease in the anode elastic constants (see Table 1).

After the cermet reduction, the fuel cell is finally connected to an external electrical circuit. The current density across the cell induces a cell warming and an inhomogeneous temperature distribution. The temperature gradient depends strongly on the stack design, the operating conditions and the gas flow configurations (cross or counter flow). It is out of the scope of this paper to deal with the effect of a potential temperature gradient on the cell stress state.

2.2.3. Stress calculation after anode re-oxidation

As mentioned above, the first reduction of the anodic cermet is accompanied by a negligible change in bulk dimension. However, if the fuel supply is stopped, the re-oxidation of the nickel phase can occur. It has been shown that this re-oxidation step generates a bulk expansion of the anodic material.[15–17] Some authors have measured this volume change using dilatometry and have shown that the expansion magnitude depends strongly on parameters such as the initial porosity,[16] the nickel content[16] or the oxidation rate of the composite.[18] As a consequence, the dimensional changes measured by the authors exhibit a substantial discrepancy. Thus, the measured anodic deformation can spread from 0% for coarse microstructure up to about 2.5% for a finer microstructure.[16]

In the present analysis, the volume expansion is considered as a parameter and its effect on cell fracture has been investigated. The re-oxidation step has been supposed to occur at a constant temperature $T = 800\,^{\circ}C$.

The stress field resulting to the cermet re-oxidation $\sigma_{ij}^{\text{re-oxidation}}$ has been calculated by adding two components:

$$\sigma_{ij}^{\text{re-oxidation}} = \sigma_{ij}^{1350\,^{\circ}C \rightarrow 800\,^{\circ}C} + \sigma_{ij}^{\text{Ni} \rightarrow \text{NiO}} \quad (1)$$

The first term $\sigma_{ij}^{1350\,^{\circ}C \rightarrow 800\,^{\circ}C}$ corresponds to the thermal residual stress calculated at the temperature of 800 °C considering the elastic constants of the oxidized NiO–YSZ cermet. The second term $\sigma_{ij}^{\text{Ni} \rightarrow \text{NiO}}$ is due to the bulk expansion of the anode. It is calculated by imposing a strain ε_{ox} to the anode layer. This variation is simulated in the finite element analysis by a thermal expansion induced by a fictive cell heating $\Delta T^{\text{fictive}}$. In order to avoid a volume variation of the cathode and electrolyte layers, their TEC are forced to 0 in this calculation step:

$$\varepsilon_{ox} = \alpha_{\text{anode}} \Delta T^{\text{fictive}} \quad (\alpha_{\text{cathode}} = \alpha_{\text{electrolyte}} = 0) \quad (2)$$

The simulations have been performed choosing the fictive cell heating in such way that the anode strain vary within the range of 0.05% to 0.3–0.4%.

Table 2
Weibull parameters of each cell material

	Weibull modulus, m	Characteristic strength, σ_0 (MPa)	Reference volume, V_0 (mm^3)
NiO–YSZ (at room temperature)[7,20]	11.8	187.0	0.578
YSZ (at room temperature)[21]	7.0	446.0	0.35
YSZ (at SOFC operating temperature)[21]	8.0	282.0	0.270
LSM (at room temperature)[7,20]	7.0	52.0	1.210
LSM (at SOFC operating temperature)[7,20]	4.0	75.0	2.810

2.3. Failure analysis methodology

The aim of this section is to present the methodology used in this work to study the mechanical cell degradation. A statistical approach has been adopted to predict the bulk failure of each cell layer (see Section 2.3.1). The method used to study the interfacial delamination between the cell layers is based on an energetic approach (see Section 2.3.2).

2.3.1. Bulk failure of the MEA layers

2.3.1.1. The Weibull approach for failure prediction. Ceramics and especially porous ceramics behave as brittle materials and exhibit a statistical strength distribution. For this reason, the Weibull approach of failure[19] has been considered to estimate the risk of rupture of each cell layer (*i.e.* the dense electrolyte and the porous electrodes). The Weibull method allows calculating the survival probability P_s of a structural component loaded with an applied tensile stress σ:

$$P_s^j(\sigma, V_j) = \exp\left(-\int_{V_j}\left(\frac{\sigma}{\sigma_0}\right)^m \frac{dV_j}{V_0}\right) \quad \text{with } j = \text{anode, electrolyte or cathode} \tag{3}$$

where V_j represents the volume of the cell layer (anode, electrolyte or cathode). The characteristic strength σ_0 represents a scale parameter for the distribution whereas the Weibull modulus m corresponds to a shape parameter. The term V_0 is a reference volume linked to the characteristic strength. The Weibull parameters for SOFC materials used in this study are listed in Table 2.

The SOFC cell structure is usually submitted to a multi-axial stress state. In this case, the total survival probability can be calculated as the product of each survival probability determined for the three principal stresses σ_i:

$$P_s^j\left(\overline{\overline{\sigma}}, V_j\right) = \prod_{i=1}^{i=3} P_s^j(\sigma_i, V_j) \quad \text{with} \quad P_s^j(\sigma_i, V_j) = \exp\left(-\int_{V_j}\left(\frac{\sigma_i}{\sigma_0}\right)^m \frac{dV_j}{V_0}\right) \tag{4}$$

This last equation assumes that the three principal stresses act independently on fracture.

2.3.1.2. Failure probability induced by the regular field. The stress field is the sum of a regular and singular component. The singular field is only dominant in a small region surrounding the singularity whereas the regular one is dominant into the remaining structure. The aim of this sub-section is to present the methodology used in this work to assess the failure risk induced by the regular field. The survival probability has been calculated with Eq. (4). The volume V_j considered for this calculation is chosen by excluding the singular volumes $V_{sing,j}$ from the volume of the whole layer $V_{tot,j}$:

$$V_j = V_{tot,j} - \sum V_{sing,j} \tag{5}$$

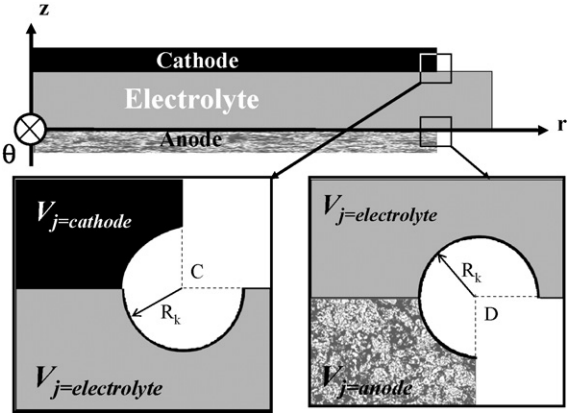

Fig. 3. Definition of the volume V_j in which the Weibull probability is calculated (case of the electrolyte-supported cell).

As illustrated in Fig. 3 for the electrolyte-supported cell, the term $V_{sing,j}$ is defined by the radius R_k corresponding to the cross-section area of the singular zone. R_k is linked to the cell geometry and can be estimated through a simple geometrical rule (see Section 4.1).

2.3.1.3. Risk of rupture initiation at singularities. The aim of this sub-section is to present the methodology used in this work to evaluate the risk of rupture initiated in the singular zone. The stress field in the vicinity of the singularities[2] (points A–D of the cell structure) is usually expressed using the local coordinates (ρ, ω) (see insets in Fig. 12):

$$\sigma_{ij} = k_1\rho^{-\lambda_1} f_{ij,1}(\omega, \varepsilon) + k_2\rho^{-\lambda_2} f_{ij,2}(\omega, \varepsilon) \quad \text{for } \rho \le R_k \tag{6}$$

where k denotes the generalized stress intensity factor, λ the singularity order and ε a parameter linked to the elastic constants mismatch for the bi-material. The subscripts 1 and 2 refer respectively to the symmetric and anti-symmetric mode of loading. This multi-parameter description of the singular stress field can be replaced by a one-parameter description on the form[22]:

$$\sigma_{ij} = k_{eq}\rho^{-\lambda_{eq}} f_{ij,eq}(\omega, \varepsilon) \quad \text{for } \rho \le R_k \tag{7}$$

k_{eq} and λ_{eq} are respectively the equivalent stress intensity factor and equivalent singularity order. It is worth noting that the stress tends to infinity when $\rho \to 0$ (the exponent λ_{eq} is higher than 0). As the stress divergence spreads on a very small region surrounding the singular point, the application of the Weibull theory requires a specific methodology which has been detailed elsewhere.[23] This methodology is based on the finite element method and allows to state if the singularity is harmful or harmless. The main steps of the procedure are the followings:

(i) The singular area is simply meshed considering an ideal shape (an ideal perpendicular corner at B or C singularity for instance).
(ii) The finite element computation is performed and the stress fields are extracted. The previous fields are integrated on each element to determine the failure probability.
(iii) The failure probability is computed again after removing from the domain of integration the first rings of elements surrounding the singularity tip and contained in the R_k radius.
(iv) If the failure probability is not sensitive to the excluded zone, it means that the couple of the singularity and the Weibull modulus is harmless: the failure probability can be directly calculated on the mesh of the whole cell layer.
(v) If the failure probability is sensitive to the excluded zone, it means that the couple of the singularity and the Weibull modulus is harmful. The probability has to be evaluated by one of the two equivalent methods:
  (a) the probability is evaluated by meshing the real notch tip radius (R_{notch}).
  (b) the survival probability can be also calculated by excluding from the domain of integration a volume smaller than the singular zone surrounding the studied singularity:

$$V_j = V_{tot,j} - V_{excluded}(R_{ex}) \quad \text{with} \quad R_{ex} < R_k \tag{8}$$

where V_j represents the volume of integration and $V_{tot,j}$ the volume of the whole cell layer. The term R_{ex} represents the radius of the cross-section corresponding to the excluded zone. It is worth noting that the size R_{ex} of this excluded zone can be linked to the radius of the notch tip R_{notch} (for a 90° notch opening angle and a Weibull modulus = 7: $R_{notch} \sim 10R_{ex}$).

2.3.2. Risk of interfacial delamination

Because of the weakness of SOFC materials, a thin layer submitted to a residual tensile stress is expected to fail by traversing cracking trough the layer thickness previous to de-bonding from its substrate. Failure at interfaces between film and substrate will happen if the film is subjected to a sufficient high compressive stress state. Indeed, the compressive stress can cause the layer to buckle from its substrate. This failure mechanism requires an initial interfacial flaw (a small region where the adhesion is poor) which can propagate when the elastic strain energy stored in the film exceeds the energy required to remove the film from its substrate (*i.e.* the interfacial toughness). If there is no interfacial defect, the delamination onset requires a second condition: a critical interfacial traction has to be applied on the interfaces.

In this work, the risk of delamination has been merely investigated by calculating the elastic strain energy stored in the compressive thin layer.

3. Calculation of the regular stress field and failure analysis

In this paragraph, the regular stress field is presented and its effect on cell mechanical failure is investigated.

3.1. Residual stress field at room temperature due to the cell elaboration

For the both axisymmetrical configurations, cooling down to the room temperature generates a uniform in-plane equi-biaxial stress state in each cell layer.

3.1.1. Stress field across the cell

3.1.1.1. Anode supported cell. The contraction of the thick anode induces a compressive stress in both electrolyte and cathode layers. This result is illustrated in Fig. 4a where the principal stress σ_r (equal to σ_θ) is plotted along the axisymmetric axis.

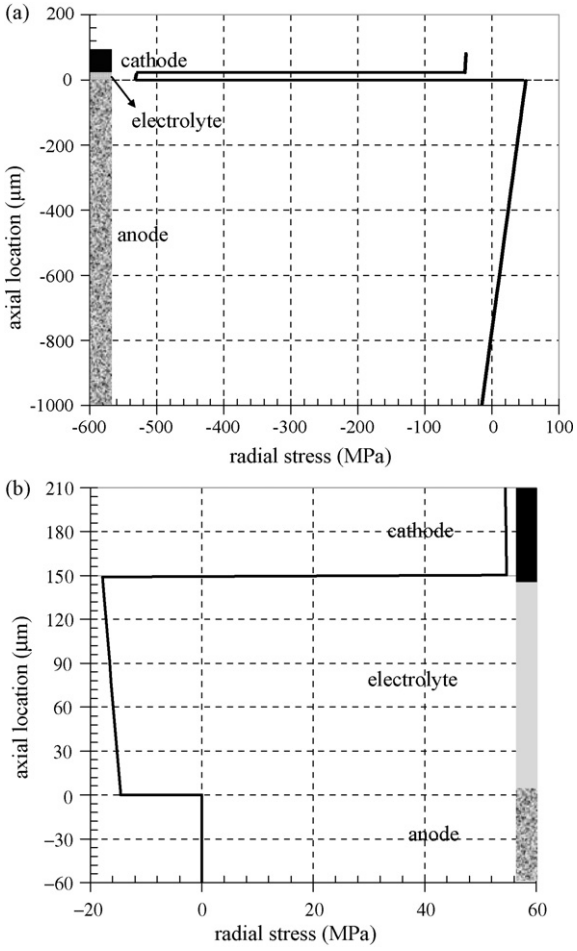

Fig. 4. Residual stress profile at room temperature across the cell. The equi-biaxial principal stress σ_r (radial stress) has been plotted as a function of the z axial location ($r = 0$): (a) anode-supported cell and (b) electrolyte-supported cell.

A slight stress gradient along this axis can be observed inside the thick cermet substrate. This gradient is linked to the cell bending and leads to a maximum tensile stress of about 50 MPa located close to the anode/electrolyte interface. The magnitude of the equi-biaxial compressive stress calculated in the electrolyte layer is about −530 MPa. This result is found to be in the same order as the stress level measured by several authors.[25,26] For instance, Fisher et al.[26] have determined a compressive stress of −560 MPa inside the YSZ layer by X-ray diffraction. This last value, slightly higher than that calculated in the present paper, can be explained by a thinner electrolyte (about 10 μm) compared to the one simulated here (20 μm).

The stress component σ_{zz} normal to the cell interfaces has been found to be close to 0 MPa. Indeed, the cell is a very thin structure in which the stress plane conditions are well verified. Moreover, the cell curvature δ remains very slight in comparison to the cell radius ($\delta/R_{cell} = 0.0126$).

3.1.1.2. Electrolyte supported cell. The elaboration of the anode/electrolyte bi-layer leads to a high equi-biaxial tensile stress in the anode layer at room temperature ($\sigma_r = \sigma_\theta \sim 286.5$ MPa at $r = 0$ mm). The NiO–YSZ cermet is not able to withstand this loading and the failure probability calculated for the anode layer reaches a value of 100%. It can be inferred from this remark that the anode layer must be completely cracked soon after its sintering onto the electrolyte.

Consequently, the account of the damaged cermet in the second step of the cell manufacturing process (*i.e.* the cathode elaboration) has been taken by considering an apparent anodic Young's modulus of 0 GPa. The simulation results show that there is again a very slight cell curvature ($\delta/R_{cell} = 0.0124$) and the stress component σ_{zz} normal to the cell interfaces is again close to 0. The equi-biaxial stress is found to be in tension in the cathode film and in compression in the electrolyte substrate (Fig. 4b).

The stress level in the cathode layer computed by using the finite element method is equal to about 54.5 MPa. It can be remarked that this value is consistent with the analytical one ($\sigma_r^{cathode} = 53.5$ MPa) determined through Eq. (9) related to the thermal residual stress in a thin film on a thick substrate[27] (ignoring any interaction with the other existing anode thin layer):

$$\sigma_r^{cathode} = \frac{(\alpha_{YSZ} - \alpha_{cathode})\Delta T}{(1 - \nu_{cathode})/E_{cathode} + ((h_{cathode}/h_{YSZ})(1 - \nu_{YSZ})/E_{YSZ})} \quad (9)$$

where α is the thermal expansion coefficient, ΔT the change in temperature, ν the Poisson's ratio and E is the Young's modulus.

3.1.2. Failure analysis due to the regular stress field

3.1.2.1. Anode supported cell geometry. Calculations have shown that the cathode and electrolyte are subjected to a compressive loading. Under this specific stress state, no extension of the ceramic defects inducing rupture is expected to occur. On the other hand, it has been also highlighted that the porous anodic cermet undergoes a tensile stress in region close to the anode/electrolyte interface. This tension leads to an anode survival probability of about 60%. In this calculation, the whole anode volume $V_{j=anode}$ has been considered in Eqs. (4) and (5). In fact, the failure risk is localised near the anode/electrolyte interface. This remark can be demonstrated by calculating the survival probability on a smaller part of the anode where the traction is the highest. This region spreads as a layer from the anode/electrolyte interface onto a distance of 20 μm inside the anodic material. Since the calculated probability value is found to be still close to 60%, it can be concluded that the possible rupture should be initiated in this particular region.

As the cathode and electrolyte thin layers are submitted to compression, the interfaces could delaminate. The strain energy stored in the cathode layer is only about 1.7 J/m^2 whereas the energy stored in the electrolyte layer reaches 20 J/m^2. This value exceeds the estimated anode/electrolyte interfacial toughness (∼10 J/m^2).[28] An interfacial flaw resulting from cell elaboration can then propagate. However, without pre-existing defects, the delamination is unlikely to be initiated because there is no residual tensile stress applied on interfaces.

3.1.2.2. Electrolyte supported cell geometry. As already mentioned, the sintering of the anode layer onto the electrolyte substrate induces a high tensile stress in the NiO–YSZ cermet. Because its survival probability falls to 0%, it can be concluded that the NiO–YSZ cermet is not able to withstand the stress induced by the manufacturing process. Therefore, the tensile stress has to be relaxed by the onset of a connected network of traversing cracks in the anode film. These conclusions are in good agreement with the experimental result of Selçuk et al.[29] Indeed, they have observed an extensive channel cracking of the NiO–YSZ anode by scanning electron microscopy (SEM).

The electrolyte substrate is subjected to a safe compressive stress state whereas the cathode thin layer undergoes a tensile equi-biaxial stress. However, the survival probability calculated for the cathode remains at 100%, and therefore, the LSM film is foreseen to bear the residual stress induced by the cell manufacturing process. This result is also in agreement with the results of Selçuk et al.[29]: the observation of cathode surfaces by SEM has revealed the absence of cracks.

Since no traversing crack is expected through the thin cathode layer, delamination between this layer and the electrolyte substrate is unlikely to occur. Furthermore, the residual tensile stress in the thin cathode allows storing only a low level of elastic energy (∼4.5 J/m^2).

3.2. Stress field during cell operation

Fig. 5a and b illustrates the evolution of the equi-biaxial stress σ_r (equal to σ_θ) in electrodes and electrolyte layers after the cell heating and after the cermet reduction.

3.2.1. Stress field after the cell heating

For both cell configurations, heating from the room temperature to SOFC operating temperature ($T = 800\,^\circ$C) lowers the stress level in each cell layer.

In the case of the anode-supported cell, the maximum tensile stress at the anode side is decreased to ∼22 MPa whereas

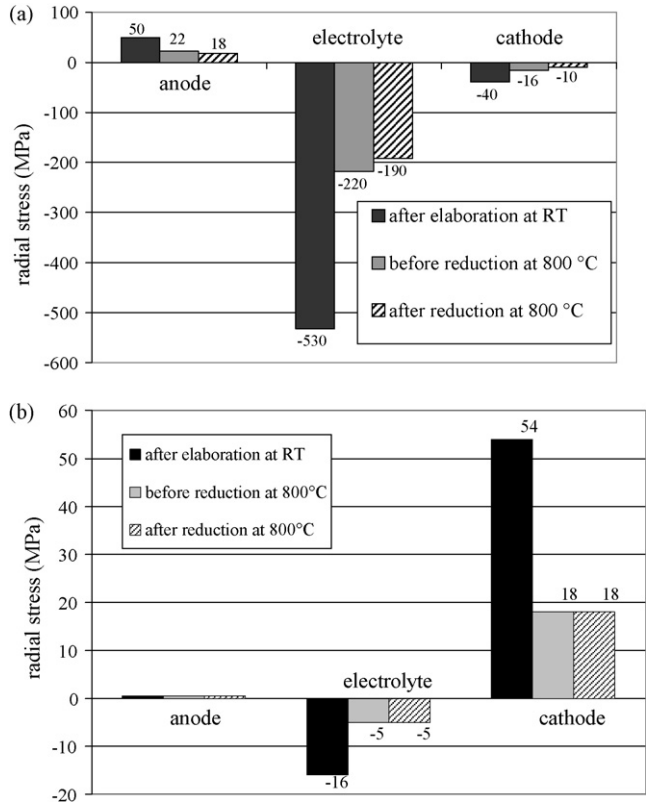

Fig. 5. Stress evolution (i) after elaboration at room temperature, (ii) before reduction at 800 °C and (iii) after reduction at 800 °C. The stress σ_r (equal to σ_θ) has been taken in the electrolyte, cathode and anode at the cell centre ($r = 0$): the given numbers correspond to the average values calculated along the axisymmetric axis excepted for the anode substrate (anode-supported cell) where the given value corresponds to the maximum tensile stress: (a) anode-supported cell and (b) electrolyte-supported cell.

the dense electrolyte and the porous electrodes remains submitted to a compressive stress (~ -220 MPa for the electrolyte and -16 MPa for the cathode). In the case of the electrolyte-supported cell, the tensile stress in cathode is lowered to $\sim$18 MPa and the electrolyte substrate remains under a slight compressive loading.

In conclusion, for the both cell configurations, heating from the room temperature to the SOFC operating one allows relaxing partially the residual stresses: under such condition, the thermal cycling between the room temperature and the SOFC operating one should not induce any cell degradation.

3.2.2. Stress field after the anode reduction

Upon NiO–YSZ reduction, the cermet Young's modulus is lowered (see Table 1). In the case of the anode-supported cell, as the anode is the thick substrate supporting the electrolyte and cathode films, its reduction tends to decrease the cell stiffness. This phenomenon leads to a stress relaxation as shown in Fig. 5a. However, this relaxation is limited: for instance, the compressive stress in the electrolyte layer is decreased from -220 to -190 MPa.

For the electrolyte-supported cell, the anode is already cracked and then the cermet reduction does not affect the apparent Young's modulus of the damaged anode. Therefore, the stress

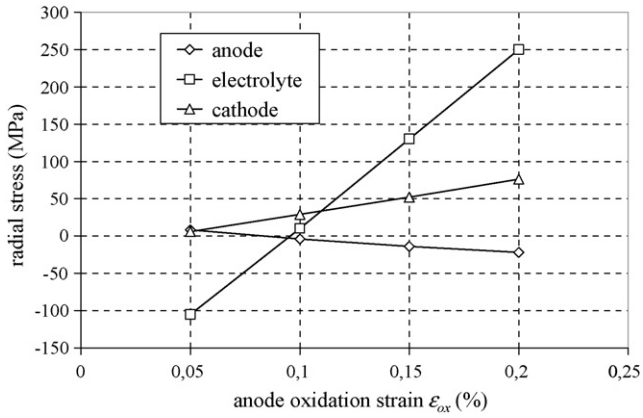

Fig. 6. Radial stress σ_r at 800 °C after the anode re-oxidation plotted as a function of the anodic strain ε_{ox} for anode, electrolyte and cathode layers (anode-supported cell).

state of the electrolyte-supported cell will not be changed after the cermet reduction.

It can be concluded from the previous result that the cermet reduction is safe and should preserve cell integrity whatever its geometry.

3.3. Stress field induced by the first re-oxidation cycle

3.3.1. Case of the anode-supported cell

3.3.1.1. Stress field after anode re-oxidation. The bulk expansion of the thick anode induces an equi-biaxial tensile stress inside the electrolyte and cathode films in addition to the initial stress field. This traction balances the initial electrolyte compressive stress as soon as the anodic volume change exceeds a strain of about 0.1% (Fig. 6). In the same time, an anode expansion equal to $\varepsilon_{ox} = 0.05\%$ is found to be sufficient to induce a tensile stress in the porous cathode.

3.3.1.2. Failure analysis. The electrolyte and cathode thin films are submitted to a tensile stress caused by the cermet re-oxidation. This loading is safe for the interfaces but could lead to the degradation of the cathode and electrolyte films.

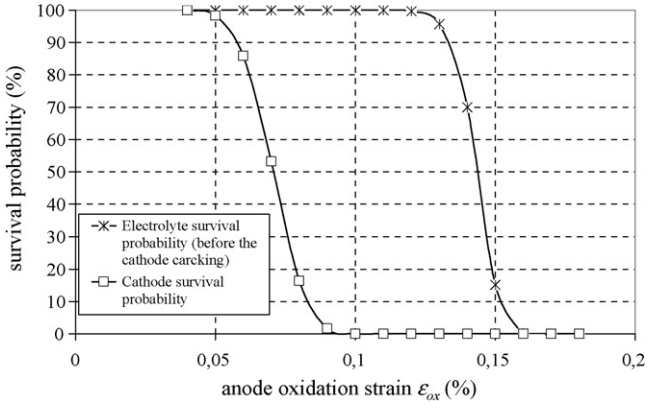

Fig. 7. Survival probability of the cathode and electrolyte films plotted as a function of the anodic strain ε_{ox} (anode-supported cell).

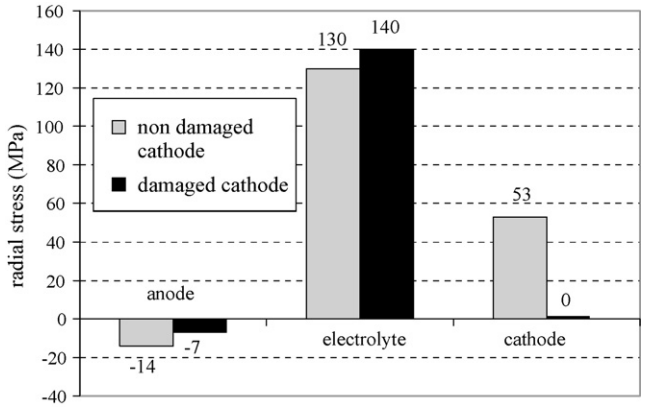

Fig. 8. Evolution of stress before and after the cathode failure (for an anodic strain of $\varepsilon_{ox} = 0.15\%$) (anode-supported cell).

The survival probability of these two thin layers has been plotted as a function of the investigated anodic strains (Fig. 7). It can be concluded from these results that the cathode layers will be damaged as soon as the anodic expansion reaches values between 0.05% and 0.09% meanwhile the electrolyte layer is predicted to fail for cermet expansion ranging from 0.12% to 0.16% (considering the undamaged cathode). This prediction is in good agreement with the result by Sarantaridis et al.[28] Indeed, they have found (by an approach based on the release of stored elastic energy) that an oxidation strain of 0.1–0.2% can be detrimental for the electrolyte integrity.

However, the cathode rupture must lead to a re-distribution of the stress state in the cell. This phenomenon has been taken into account in the calculations by forcing the cathode Young's modulus to tend to 0 GPa (as soon as the cathode has failed). As illustrated in Fig. 8, the level of stress in the electrolyte layer is found to be increased slightly while the cathode loading falls to 0. Therefore, the cell stress re-arrangement due to the cathode failure induces a slight decrease of the electrolyte survival probability (Fig. 9): the electrolyte fracture is foreseen to occur for anodic expansion ranging between 0.12% and 0.15%.

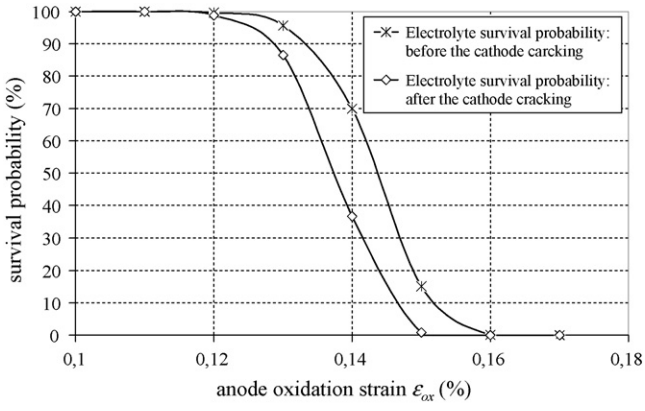

Fig. 9. Survival probability of the electrolyte plotted as a function of the anodic strain ε_{ox} calculated before and after the cathode cracking (anode-supported cell).

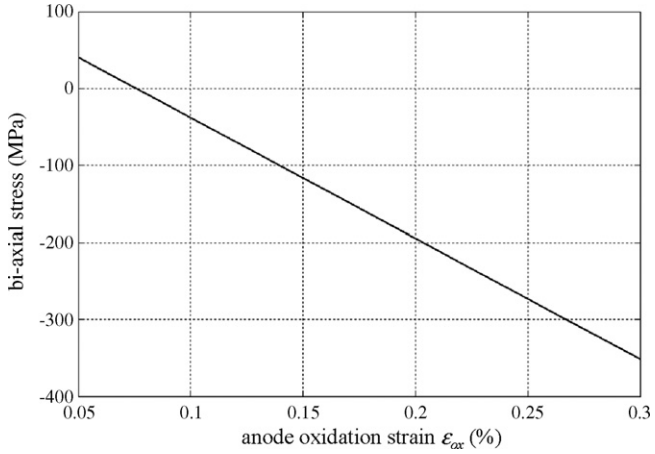

Fig. 10. Stress induced in the anode layer as a function of the cermet oxidation strain ε_{ox} (electrolyte-supported cell).

3.3.2. Case of the electrolyte-supported cell

3.3.2.1. Stress field after anode re-oxidation. As mentioned in the Section 3.1.2, the elaboration of the anode layer leads to its degradation into a connected network of cracks surrounding islands of intact film. For instance, the observations carried out by Selçuk et al.[29] on thin layers of NiO–YSZ cermet have shown that, in their case, the crack separation was about 200 μm. In order to investigate the effect of the anode re-oxidation, the local stress inside these islands has been estimated. Considering the elastic parameters of the un-damaged cermet and neglecting the stress relaxation in the vicinity of the anodic cracks, the equi-biaxial stress in the middle of the islands remains described by the Eq. (1): the stress field is the sum of one contribution due to the thermal residual stress and one contribution caused by the cermet bulk expansion. In this approach, the thermal residual stress in island will be taken equal to its maximum expectable value before cracking.

In Fig. 10, the calculated stress after the re-oxidation has been plotted as a function of the anode expansion. It can be seen that the thin layer is subjected to a compressive stress field as soon as the anode strain is higher than $\varepsilon_{ox} \sim 0.07\%$.

3.3.2.2. Failure analysis. Because of the biaxial compressive stress state, the un-cracked islands of anodic film could delaminate. Fig. 11 shows the evolution of the energy stored in these islands as a function of the cermet strain ε_{ox}. In our case (for an anode thickness of 60 μm), the estimated interfacial toughness ($\sim 10\ J/m^2$)[28] is expected to be overtaken as soon as the anodic strain is equal to $\varepsilon_{ox} \sim 0.18\%$.

4. Effect of singularities on the cell degradation

4.1. Singular stress field and k-dominance radius

The local coordinates (ρ, ω) related to each cell singularities (points A–D in Fig. 1) have been used to express the singular fields. The logarithm of the simulated hoop stress $\sigma_{\omega\omega}$ has been plotted as a function of the distance from the singularity tip along the interface (*i.e.* for $\omega = 0°$). These curves have been

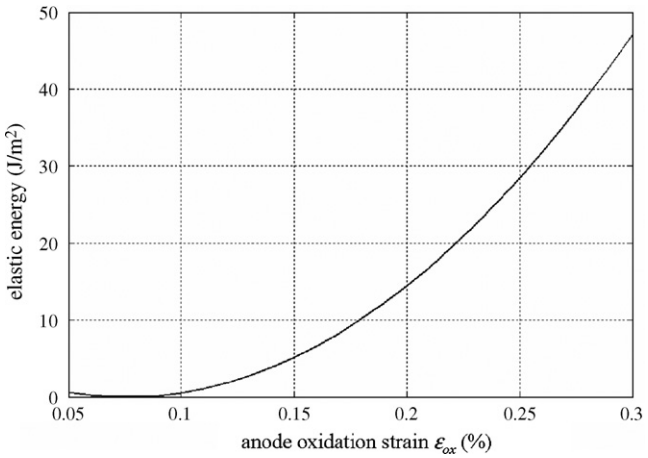

Fig. 11. Elastic energy stored in the anode layer after its re-oxidation (electrolyte-supported cell).

established for each investigated cell loading (*i.e.* the residual stresses at room temperature, during cell operation and after the anode re-oxidation). As an illustration in Fig. 12a and b, the residual stress components $\sigma_{\omega\omega}$ after the cell elaboration has been plotted in the neighbourhood of the singularities A and C for anode and electrolyte supported cells, respectively.

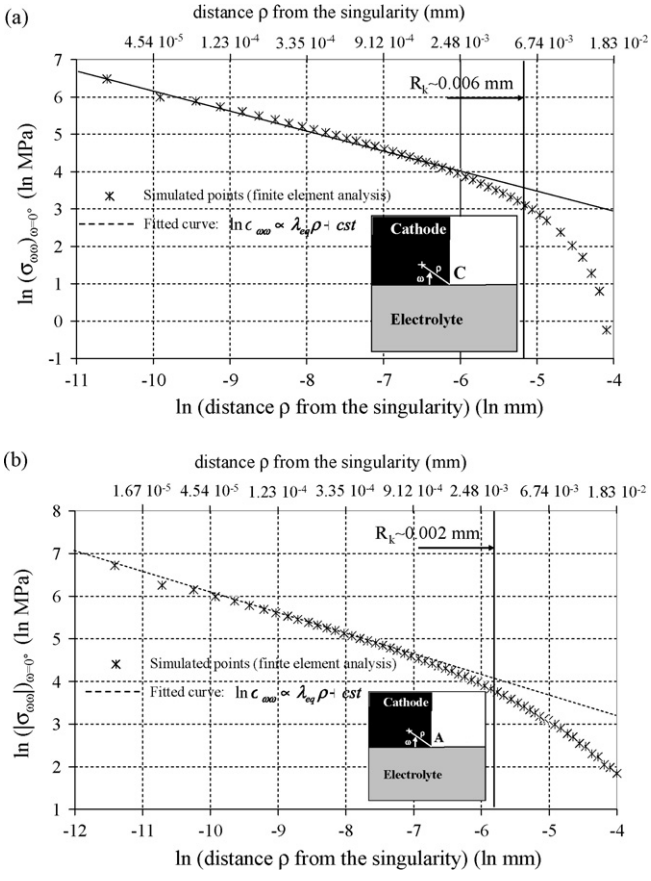

Fig. 12. In the local coordinates (ρ, ω) of the singularity, the logarithm of the $\sigma_{\omega\omega}$ stress due to the cell manufacturing process has been plotted as a function of the distance from the singularity tip (along the interface: $\omega = 0°$): (a) singularity C of the electrolyte-supported cell and (b) singularity A of the anode-supported cell.

According to Eq. (7), the linear part of the curve defines the *k*-dominance radius R_k in which the fields are governed by the singularity. In all investigated cases, it has been found that the *k*-dominance radius is about $R_k \sim 2$ μm for the anode supported cell configuration and $R_k \sim 6$ μm for electrolyte supported cell configuration. Therefore, it can be concluded that the radius R_k may be taken as one tenth of a length *L*, defined as the shortest of the cell layer thicknesses:

$$R_k = \frac{L}{10} \tag{10}$$

where *L* is either equal to the electrode thickness (60 μm) for the electrolyte-supported cell or equal to the electrolyte thickness (20 μm) in the case of the anode-supported cell. This result is consistent with the rule mentioned by O'Dowd and Shih for interfacial cracks.[30]

4.2. Failure analysis due to the singular stress field

The methodology summarized in Section 2.3.1 has been applied to the singularities of the both cell geometries: the survival probabilities have been calculated for each cell layer by excluding a small volume surrounding the studied singularity.

4.2.1. Singularity A and B of the anode-supported cell geometry

4.2.1.1. Effect of the pure material singularity B. Considering the anodic substrate, it is shown that the survival probability is not changed when the singular volume surrounding the singularity B is taken into account in the calculation. This result is illustrated in Fig. 13 considering the residual stress at room temperature. The same result has been highlighted for the electrolyte substrate. Even for a cell loading after anode re-oxidation, the risk of electrolyte fracture is not increased by taking into account the singular volume. It means that the pure material singularity B is harmless for both the anode substrate and the electrolyte layer. Therefore, the Weibull approach to predict the rupture can be directly applied on the whole cell layer. In other words, even if the level of stress is sufficiently high to obtain a high failure probability, the local risk of rupture is not higher in the singular zone than in the remaining cell volume.

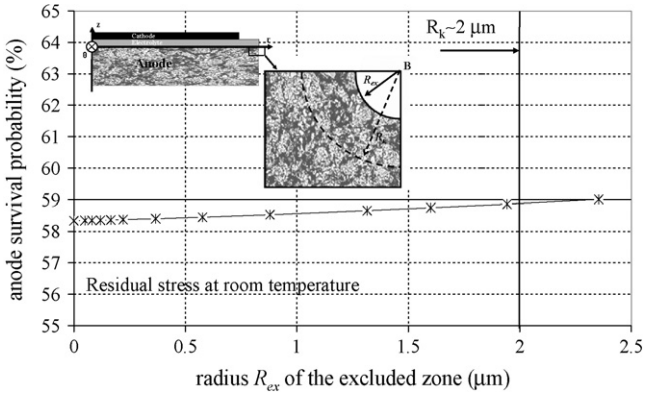

Fig. 13. Survival probability of the anode substrate calculated by removing from the domain of integration a region surrounding the singularity B (case of the residual stress at room temperature).

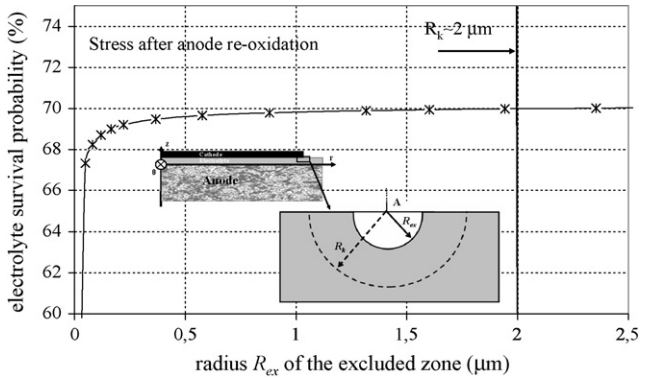

Fig. 14. Survival probability of the electrolyte substrate calculated by removing from the domain of integration a region surrounding the singularity A (case of the stress after anode re-oxidation with a bulk expansion of $\varepsilon_{ox} = 0.14\%$ and an un-cracked cathode).

4.2.1.2. Effect of the geometrical and material singularity A. The geometric and material singularity A is found to be harmless for the cathode layer. However, the survival probability calculated at the electrolyte side exhibits a dependence on the radius of the excluded zone surrounding the singularity. It means that the singularity A is potentially harmful for the electrolyte layer. The Weibull approach to predict the rupture cannot be directly applied on the whole electrolyte volume: a small zone surrounding the singularity has to be removed.

In the case of the residual stress at room temperature and during cell operation, the electrolyte stress state is found to be in such configuration that the rupture is not expected to be initiated at the singularity A. Indeed, a radius of the excluded zone R_{ex} smaller than 0.05 µm is sufficient to obtain an electrolyte survival probability of 100%. This condition corresponds to a radius of the notch (singularity) tip R_{notch} larger than ~0.5 µm (according to the relation $R_{notch} \sim 10R_{ex}$ given in Section 2.3.1). Practically, the real notch tip must fulfil this requirement.

However, for the electrolyte loading due to the anode re-oxidation, the electrolyte survival probability is clearly dependent on the size of the excluded zone surrounding the singularity (Fig. 14): the notch tip radius has to be determined precisely. If this radius is lower than ~5 µm, an electrolyte rupture initiation (from singularity A) appears to be possible.

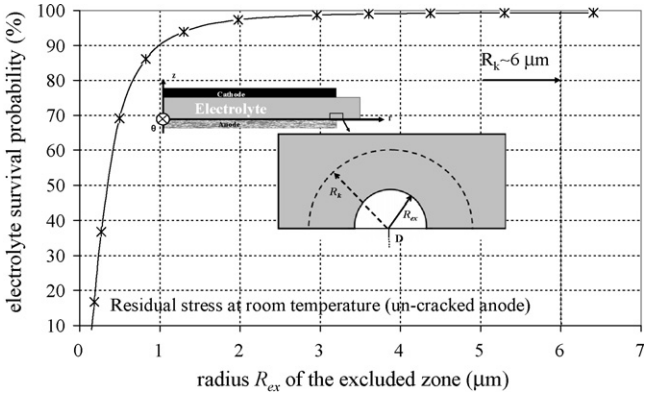

Fig. 15. Survival probability of the electrolyte substrate calculated by removing from the domain of integration a region surrounding the singularity D (case of the residual stress at room temperature and for an un-cracked anode).

4.2.2. Singularity C and D of the electrolyte-supported cell geometry

4.2.2.1. Effect of the geometrical and material singularity D. The anode survival probability is found to be independent of the size of the excluded zone in the vicinity of the singularity D. This singularity is then completely safe for the anode layer.

At the opposite side, the electrolyte survival probability is found to be strongly dependent on the excluded zone surrounding the singularity. This result is illustrated in Fig. 15 where the electrolyte survival probability has been plotted as a function of the size of the excluded zone for the residual stress at room temperature and considering the un-cracked anode. Therefore, the electrolyte fracture can be easily initiated by the YSZ flaws contained in the singular region. If the anode material resists to thermal stress during the cooling from its sintering temperature, the risk to initiate the electrolyte degradation from the singularity A is very high.

4.2.2.2. Effect of the geometrical and material singularity C. The point C for electrolyte-supported cell represents the same singularity as A for the anode-supported cell (since the singularity is completely defined by the 90° notch opening angle at the cathode/electrolyte free edge and by the LSM/YSZ couple of materials). Therefore, the conclusions established for the singular point A of the anode supported cell remains valid for the present singularity: it is harmless for the porous cathode and potentially harmful for the dense electrolyte.

5. Discussion

5.1. Anode-supported cell

It has been demonstrated that the thermal residual stress at room and operating temperatures should not induce any significant mechanical damage of the dense electrolyte. However, a tensile stress has been highlighted in the porous anode close to the anode/electrolyte interface. In our reference geometry and with the Weibull parameters given in Table 2, the tensile stress induces an anode survival probability of 60%. It is worth to underline that other Weibull parameters are available in the lit-

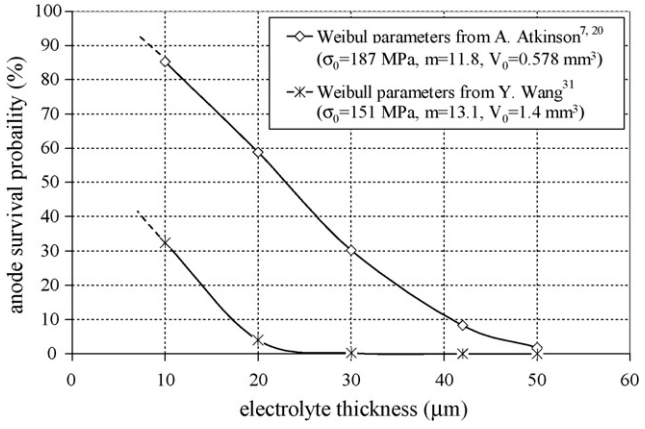

Fig. 16. Anode survival probability at room temperature plotted as a function of the electrolyte thickness (resulting from the elaboration stress).

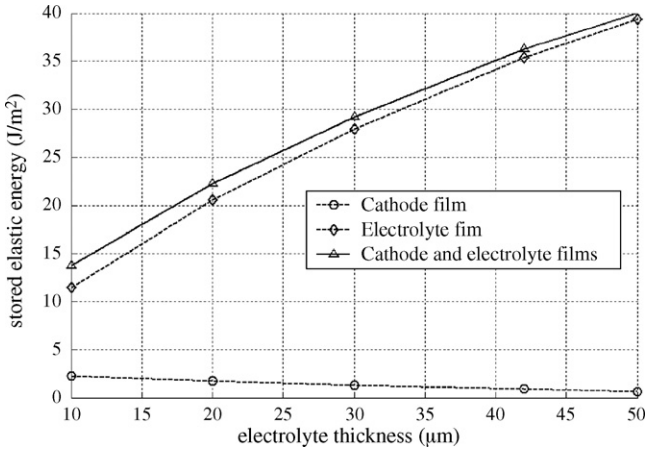

Fig. 17. Elastic energy stored in the electrolyte layer plotted as a function of its thickness (resulting from the elaboration stress).

erature and are related to different cermet microstructures.[4,31] Changing these parameters can substantially shift the survival probability. However, the trends with the cell geometrical dimensions remain unchanged: this point is illustrated in Fig. 16 where the impact of the electrolyte thickness on the risk of anode failure has been investigated for two sets of Weibull data.[7,31]

In Fig. 16, it can be noticed that the anode survival probability is increased when the electrolyte thickness is decreased. This trend is a consequence of the decrease of the anode tensile stress when decreasing the electrolyte thickness.

The elaboration of the anode-supported cell leads to a high compressive stress in the electrolyte and cathode thin layers. Because of the high energy stored in these layers, the interfaces will be able to delaminate as soon as they will be subjected to a tensile stress (by cell bending for instance). However, this risk can be lowered by decreasing the electrolyte thickness. Indeed, the energy stored in the electrolyte layer at room temperature is decreased with decreasing its thickness (Fig. 17).

In our reference geometry, it has been found that, upon cermet re-oxidation, a very low anode strain is sufficient to cause the cathode failure. Indeed, the risk of rupture reaches 100% for an anodic bulk strain of about 0.09%. Under such conditions, regarding usual cermet bulk expansion, it seems difficult to avoid the cathode degradation. The electrolyte failure has been foreseen to occur for an anode expansion of about 0.12–0.15%. As the electrolyte fracture leads to the fatal loss of the cell open circuit voltage, the anodic bulk deformations have to remain under these limit values. The cell mechanical failure during the cermet re-oxidation is also influenced by the electrolyte thickness as illustrated in Fig. 18: the thinner is the dense electrolyte, the higher is its survival probability. Indeed for the thin layers, the risk to have a critical defect is sufficiently low to avoid the rupture (because of the small volume) in spite of a high level of stress. However, it is worth noting that for very thin electrolyte, other mechanisms could be involved in the film rupture that forbids any extrapolation of the present results.

In conclusion, for the case of an anode-supported cell, an electrolyte ranging around 10 μm thickness seems to constitute a good compromise to withstand the redox cycles and to limit the risk of anode damage and anode/electrolyte delamination.

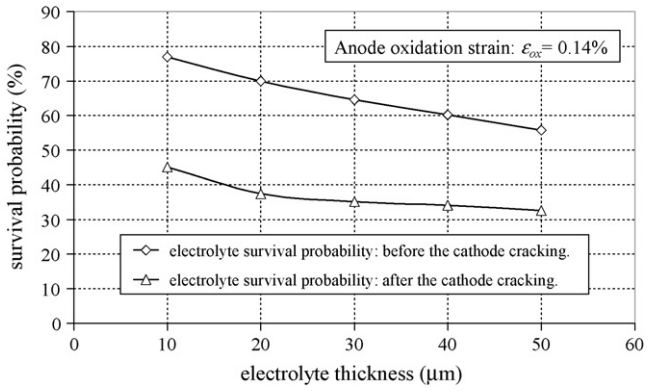

Fig. 18. Electrolyte survival probability calculated after the anode re-oxidation (ε_{ox} = 0.14%) and plotted as a function of the electrolyte thickness.

5.2. Electrolyte-supported cell

The simulations have shown that the thin anode layer is not able to withstand the equi-biaxial stress caused by the manufacturing process. The occurrence of an extensive channel cracking is then unavoidable. It is worth to underline that the anode degradation could only have an impact on its electrochemical efficiency (the cell continues to operate as the electrolyte and interfaces are not damaged).

More embarrassing is the risk of delamination due to the anode re-oxidation. Fortunately, the elastic energy stored in the islands of intact cermet is found to decrease with decreasing the anode thickness (Fig. 19). Then, considering a 10 μm anode thickness, the elastic energy stored in the cermet film reaches the anode/electrolyte estimated interfacial toughness (~10 J/m^2) for an anodic expansion of about 0.35%. In conclusion, the risk of delamination is lowered when decreasing the anode thickness. But, on the other hand, a minimal thickness is required to ensure an efficient current collection and therefore, a compromise on the anode thickness has to be found.

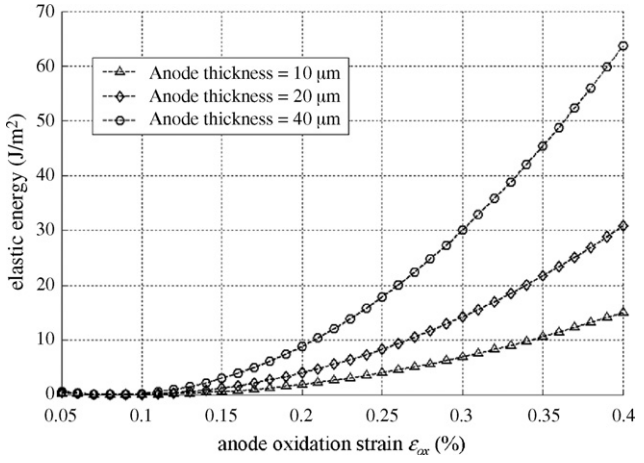

Fig. 19. Elastic energy stored in the anode layer plotted as a function of its strain after re-oxidation.

5.3. Comparison of the anode and electrolyte-supported cell robustness

From the present analysis, it appears that the robustness of the electrolyte-supported cell is much better than the anode-supported cell. Indeed, the strength of the dense YSZ is obviously higher than the strength of the porous cermet. In addition, at room temperature, the risk to delaminate the interfaces is much higher in the case of the anode-supported cell than in the case of the electrolyte-supported cell.

Upon cermet re-oxidation, even a low bulk expansion of the thick anodic substrate is sufficient to involve the electrolyte cracking. In the case of the electrolyte-supported cell, the failure mechanism after the redox cycle corresponds to the YSZ/NiO–YSZ interfacial failure. However, this delamination is expected to occur for higher value of anodic expansion in comparison to the one involved in the anode-supported cell rupture.

In spite of its mechanical weakness, the anode-supported cell presents the smallest area specific resistances (ASR). These good electrochemical performances are mainly explained by the thin electrolyte which minimizes the ionic losses during operation. Furthermore, the anode degradation of the electrolyte-supported cell could damage the electrochemical functional layer in such way that the density of three-phase boundaries (TPBs) is decreased. Therefore, for a given microstructure, the anodic activation over-potential could be higher in the case of the electrolyte-supported cell than for the anode-supported cell. In addition, the current collection could be hindered by the presence of cracks in the thin anode.

5.4. Geometrical impact of singularities on cell robustness

It has been demonstrated in Section 4.2 that the pure cell material singularity (defined by the bi-material and by the electrode/electrolyte straight free edge) is harmless for the cell integrity.

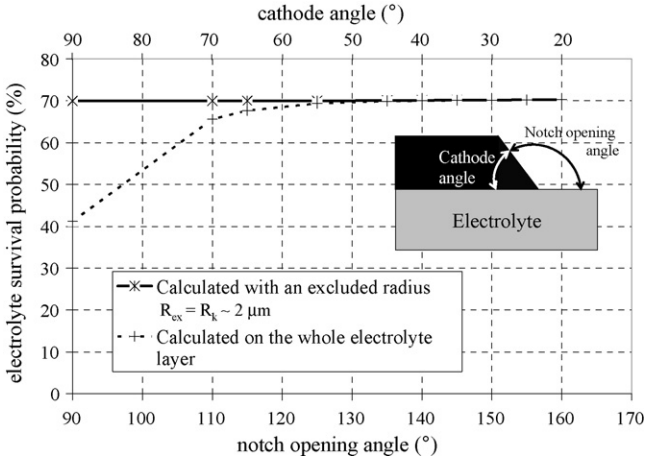

Fig. 20. Electrolyte survival probability plotted as a function of cathode angle. The solid line corresponds to the probability calculated with the regular field (by excluding the singular zone) and the dashed line corresponds to the probability calculated on the whole layer (anode-supported cell, stress state after re-oxidation, $\varepsilon_{ox} = 0.14\%$).

On the contrary, the geometrical and material singularity (defined by the bi-material and by the 90° notch opening angle at the electrode/electrolyte free edge) is potentially harmful. In this case, it has been shown that the degradation can be initiated in the vicinity of the singularity on the side of the dense electrolyte. Various kinds of geometrical modifications may be proposed to remove the risk of rupture initiated in such singularities:

- If the electrodes cover the whole electrolyte surface, the cell singularities will be reduced to the harmless bi-material effect.
- The singularities can be completely erased by controlling the electrode angle: for instance, in Fig. 20, the cathode angle has been decreased and its impact on the electrolyte survival probabilities has been investigated. As soon as the cathode angle is lowered from 90° to 50°, the probability determined with the both singular and regular field (dashed line) reaches the probability calculated by taken into account only the regular field (solid line). It means that the 50° angle is sufficiently low to completely remove the risk of failure due to the singularity.

6. Conclusion

A numerical tool has been developed to study the risk of cell failure due to the residual stress arising (i) after the manufacturing process, (ii) at SOFC operating temperature, and (iii) after the anode re-oxidation. Considering the usual materials employed for the MEA, this methodology has been applied to the two classical planar cell configurations:

(i) The elaboration of the electrolyte-supported cell induces a residual stress state leading to the extensive channel cracking of the anode layer. The cathode and electrolyte layers are predicted to be safe.

In the case of the anode-supported cell, an optimized electrolyte thickness around 10 μm seems sufficient to avoid any degradation. However, the high compressive stress in the thin electrolyte and cathode layers leads to a high stored elastic energy. This energy will build up the driving force for delamination if a tensile stress is applied on the interfaces (for instance, when the cell is set up in a stack).

(ii) The stress field at SOFC operating temperature has been calculated before and after the cermet reduction. In both cases and for both cell configurations, it has been shown that the stress level inside the cell is partially relaxed. Under such conditions, the thermal cycling between the room temperature and the SOFC operating temperature should not induce any cell degradation.

(iii) The first cermet re-oxidation step has also been analyzed. The stress calculations have been performed for various anodic volume expansions. In the case of the anode-supported cell, it has been shown that the cathode is damaged as soon as the anodic strain reaches values between 0.05% and 0.09%. The electrolyte fracture has been predicted to occur for anodic expansion ranging between 0.12% and 0.15%. For the electrolyte-supported cell, the cermet oxidation induces a risk of

anode/electrolyte interfacial fracture. In the case of a 10 μm anode thickness, an anodic strain lower than 0.3–0.35% is recommended to avoid the delamination.

A special attention has been paid to the cell rupture initiated from the singularities. By using an appropriate methodology presented elsewhere, it has been shown that the pure electrode/electrolyte singularity is harmless. The perpendicular corner at the electrode/electrolyte free edge constitutes a harmful singularity. In this case, it has been shown that the rupture will be initiated in the vicinity of the singularity on the electrolyte side. Some cell geometrical improvements have been proposed to modify these singularities in order to limit their impact on fracture and increase the cell reliability.

Acknowledgments

The authors would like to thank Dr. J. Mougin for many useful discussions and the critical reading of the manuscript. Part of this work has been obtained in the framework of the research program called CIEL, led by Mr. S. Hody from Gaz de France and supported by the French National Research agency ANR (contract number ANR-05-PanH-024).

References

1. Singhal, S. C. and Kendall, K., In *High Temperatures Solid Oxide Fuel Cells*, ed. S. C. Singhal and K. Kendall. Elsevier, Oxford, 2003, pp. 5–10.
2. Leguillon, D. and Sanchez-Palencia, E., *Computation of Singular Solutions in Elliptic Problems and Elasticity*. J. Wiley and Masson, New York, Paris, 1987.
3. http://www-cast3m.cea.fr/cast3m/index.jsp.
4. Radovic, M. and Lara-Curzio, E., Mechanical properties of tape cast nickel-based anode materials for solid oxide fuel cells before and after reduction in hydrogen. *Acta Mater.*, 2004, **52**, 5747–5756.
5. Radovic, M. and Lara-Curzio, E., Elastic properties of nickel-based anodes for solid oxide fuel cells as a function of the fraction of reduced NiO. *J. Am. Ceram. Soc.*, 2004, **87**(12), 2242–2246.
6. Tietz, F., Thermal expansion of SOFC materials. *Ionics*, 1999, **5**, 129–139.
7. Atkinson, A. and Selçuk, A., Mechanical behaviour of ceramic oxygen ion-conducting membranes. *Solids State Ionics*, 2000, **134**, 59–66.
8. Aruna, S. T., Muthuraman, M. and Patil, K. C., Synthesis and properties of Ni–YSZ cermet: anode material for solid oxide fuel cells. *Solids State Ionics*, 1998, **111**, 45–51.
9. Nishikawa, T., Ogawa, D., Honda, S. and Awaji, H., Mechanical and electrical properties of porous lanthanum strontium manganite at operating temperature. *J. Soc. Mater. Sci. (Jpn.)*, 2003, **52**(6), 587–591.
10. Fehringer, G., Janes, S., Wildersohn, M. and Clasen, R., Proton-conducting ceramics as electrode/electrolyte—materials for SOFCs: preparation, mechanical and thermal–mechanical properties of thermal sprayed coatings, material combination and stacks. *J. Eur. Ceram. Soc.*, 2004, **24**, 705–715.
11. Nakajo, A., Stiller, C., Härkegard, G. and Bolland, O., Modelling of thermal stresses and probability of survival of tubular SOFC. *J. Power Sources*, 2006, **158**, 287–294.
12. McEvoy, A., In *High Temperatures Solid Oxide Fuel Cells*, ed. S. C. Singhal and K. Kendall. Elsevier, Oxford, 2003, p. 154.
13. Yokokawa, H. and Horita, T., In *High Temperatures Solid Oxide Fuel Cells*, ed. S. C. Singhal and K. Kendall. Elsevier, Oxford, 2003, p. 142.
14. Jorgensen, M. J. and Mogensen, M., Impedance of solid oxide fuel cell LSM/YSZ composite cathodes. *J. Electrochem. Soc.*, 2001, **148**(5), A433–A442.
15. Klemenso, T., Chung, C., Larsen, P. H. and Mogensen, M., The mechanism behind redox instability of anodes in high-temperature of SOFCs. *J. Electrochem. Soc.*, 2005, **152**(11), A2186–A2192.
16. Waldbillig, D., Wood, A. and Ivey, D. G., Thermal analysis of the cyclic reduction and oxidation behaviour of SOFC anodes. *Solids State Ionics*, 2005, **176**, 847–859.
17. Cassidy, M., Lindsay, G. and Kendall, K., The reduction of nickel–zirconia cermet anodes and the effects on supported thin electrolytes. *J. Power Sources*, 1996, **61**, 189–192.
18. Stathis, G., Simwonis, D., Tietz, F. and Moropoulou, A., Oxidation and resulting mechanical properties of Ni/8Y_2O_3-stabilized zirconia anode substrate for solid oxide fuel cells. *J. Mater. Res.*, 2002, **17**(5), 951–958.
19. Weibull, W., A statistical distribution function for wide applicability. *J. Appl. Mech.*, 1951, **18**(3), 293–297.
20. Atkinson, A. and Selçuk, A., Mechanical properties of ceramic materials for solid oxide fuel cells. In *Proceedings of the 5th International Symposium on SOFC (SOFC V), Electrochemical Society, vols. 97–81*, 1997, pp. 671–680.
21. Selçuk, A. and Atkinson, A., Strength and toughness of tape-cast yttria stabilized zirconia. *J. Am. Ceram. Soc.*, 2000, **83**(8), 2029–2035.
22. Towse, A., Potter, K. D., Wisnom, M. R. and Adams, R. D., The sensitivity of a Weibull failure criterion to singularity strength and local geometry variations. *Int. J. Adhes. Adhes.*, 1999, **19**, 71–87.
23. Laurencin, J., Delette, G. and Dupeux, M., An estimation of ceramic fracture at singularities by a statistical approach. *J. Eur. Ceram. Soc.*, 2007, **28**, 1–13.
25. Yakabe, H., Baba, Y., Sakurai, T., Satoh, M., Hirosawa, I. and Yoda, Y., Evaluation of residual stresses in a SOFC stack. *J. Power Sources*, 2004, **131**, 278–284.
26. Fisher, W., Malzbender, J., Blass, G. and Steinbrech, R. W., Residual stresses in planar solid oxide fuel cells. *J. Power Sources*, 2005, **150**, 73–77.
27. Clyne, T. W., In *Encyclopaedia of Materials: Science and Technology*, ed. P. J. Withers. Elsevier, 2001, pp. 8126–8134.
28. Sarantaridis, D. and Atkinson, A., Mechanical modeling of redox cycling damage in solid oxide fuel cells. In *Proceedings of the 7th European Fuel Cell Forum*, 2006.
29. Selçuk, A., Merere, G. and Atkinson, A., The influence of electrodes on the strength of planar zirconia solid oxide fuel cells. *J. Mater. Sci.*, 2001, **36**, 1173–1182.
30. Shih, C. F., Cracks on bimaterial interfaces: elasticity and plasticity aspects. *Mater. Sci. Eng.*, 1991, **A143**, 77–90.
31. Wang, Y., Walter, M. E., Sabolsky, K. and Seabaugh, M. M., Effects of powder sizes and reduction parameters on the strength of Ni–YSZ anodes. *Solids State Ionics*, 2006, **177**, 1517–1527.